

1 **Identifying Prepubertal Children with Risk for Suicide Using Deep**  
2 **Neural Network Trained on Multimodal Brain Imaging-Derived**  
3 **Phenotypes**

4

5 **Bo-Gyeom Kim<sup>1\*</sup>, Gun Ahn<sup>2\*</sup>, Sooyoung Kim<sup>3\*</sup>, Kakyeong Kim<sup>3</sup>, Hyeonjin Kim<sup>1</sup>,**  
6 **Eunji Lee<sup>1</sup>, Woo-Young Ahn<sup>1,3,5</sup>, Jae-Won Kim<sup>4</sup>, Jiook Cha<sup>1,3,5</sup>**

7 1. Department of Psychology, College of Social Sciences, Seoul National University

8 2. Interdisciplinary Program in Bioengineering, College of Engineering, Seoul  
9 National University

10 3. Department of Brain and Cognitive Sciences, College of Natural Sciences, Seoul  
11 National University

12 4. Division of Child and Adolescent Psychiatry, Seoul National University Hospital

13 5. AI Institute, Seoul National University

14 \* denotes equal contribution.

15

16 **Correspondence to:**

17 Jiook Cha, PhD

18 Gwanak-ro 1, Building #16, Suite M512

19 Gwanak-gu, Seoul, Republic of Korea

20 [connectome@snu.ac.kr](mailto:connectome@snu.ac.kr)

## 21            **Abstract**

22            Suicide is among the leading causes of death in youth worldwide. Early identification  
23 of children with high risk for suicide is key to effective screening and prevention strategies.  
24 Brain imaging can show functional or structural abnormalities related to youth suicidality, but  
25 literature is scarce. Here we tested the extent to which brain imaging is useful in predicting  
26 suicidal risk in children. In the largest to date, multi-site, multi-ethnic, epidemiological  
27 developmental samples in the US (N = 6,172; the ABCD study), we trained and validated  
28 machine learning models and deep neural networks on the multimodal brain imaging derived  
29 phenotypes (morphometry, white matter connectivity, functional activation, and connectivity)  
30 along with behavioral and self-reported psychological questionnaire data. The model trained  
31 on diffusion white matter connectomes showed the best performance (test AUC-ROC = 74.82)  
32 with a one percentage increase compared with the baseline model trained on behavioral and  
33 psychological data (test AUC-ROC = 74.16). Models trained on other MRI modalities showed  
34 similar but slightly lower performances. Model interpretation showed the important brain  
35 features involved in attention, emotion regulation, and motor coordination, such as the anterior  
36 cingulate cortex, temporal gyrus, and precentral gyrus. It further showed that the interaction  
37 of brain features with depression and impulsivity measures contributed to the optimal  
38 prediction of youth suicidality. This study demonstrates the potential utility of a multimodal  
39 brain imaging approach to youth suicidality prediction and uncovers the relationships of the  
40 psychological and multi-dimensional and multi-modal neural features to youth suicidality.

## 41 Introduction

42 Suicide is a major public health problem, with more than 25 million suicide attempts  
43 occurring each year worldwide. In youth, suicide is among the leading causes of death. Most  
44 suicide research focuses on the adult population <sup>1</sup>, and the literature on youth suicidality has  
45 been scarce. Identifying the neural underpinnings of youth suicidality will advance research  
46 by allowing brain-based markers and targets for prediction, monitoring and prevention <sup>2</sup>. Also,  
47 early detection of youth suicidality may not only prevent death by suicide among children but  
48 also reduce the risk of psychopathology later in life.

49 Prior brain imaging literature suggests a link between youth suicidality and abnormally  
50 delayed neurocognitive development. Children with suicidal ideation showed a reduced brain  
51 response to reward <sup>3</sup> or decreased cognitive capacity <sup>4</sup>. As abnormal neurocognitive  
52 development may cause long-term sequelae, young children with prior suicide ideation are  
53 more likely prone to the risk for suicide in their later life.

54 Based on recent findings of brain abnormalities linked to suicidality, several studies  
55 applied machine learning to brain imaging data in small samples. Gosnell et al. classified  
56 suicidal psychiatric inpatients and non-suicidal inpatients with resting-state functional  
57 connectivity and structural neuroimaging<sup>5,6</sup>. Just et al. demonstrated that the functional  
58 coupling of the brain regions like the superior medial frontal and anterior cingulate regions,  
59 during death-related and life-related concepts, could identify youth with suicidal ideation <sup>7</sup>.  
60 Although previous studies show promise, the practical utility of neuroimaging-based prediction  
61 of youth suicidality remains untested rigorously in sufficiently large, representative samples  
62 using rigorous predictive modeling approaches.

63 Multimodal data integration may help predict. Combining the brain's structural and  
64 functional aspects, multimodal brain imaging may better account for complex and dimensional  
65 brain abnormalities related to suicidality compared with a single modality approach <sup>8</sup>. No

66 literature in suicidality research, however, has provided information of what combinations of  
67 imaging modalities would optimally explain brain abnormalities related to youth suicidality.

68         Here, we aim to identify youth with suicidal ideation using deep learning trained on the  
69 brain structural, functional, and connectivity data, as well as behavioral and psychological  
70 measures. Beyond prediction, using interpretable deep learning, we aim to identify brain circuit  
71 features and psychological measures of which nonlinear interactions may contribute to  
72 prediction. Leveraging large, representative, epidemiological, multi-site, and developmental  
73 study in the US, we test the generalizability and practicality of the prediction models. We also  
74 test the utility of advanced computational learning strategies, such as stacking ensembles for  
75 data integration and GANs for data augmentation in psychiatric research.

## 76 **Methods**

### 77 **Study Sample**

78 The Adolescent Brain and Cognitive Development (ABCD) study recruited a nationally  
79 representative cohort of 9- and 10-year-old children from 21 research sites across the US <sup>4</sup>.  
80 For the current analysis, we used minimally preprocessed data from the curated ABCD annual  
81 release 2.0.1 and selected ABCD participants based on the availability of non-imaging  
82 measures and neuroimaging data. The number of participants was different in each dataset:  
83 sMRI, dMRI, and rs-fMRI dataset included 5,878 participants (783 cases and 5044 controls  
84 for suicidal ideation; 48 cases and 5779 controls for suicidal attempt). SST fMRI, N-back fMRI,  
85 and MID fMRI included (592 cases and 4035 controls for suicidal ideation; 34 cases and 4596  
86 controls for suicidal attempt). Thus, total participants consisted of 6,172 children (837 cases  
87 and 5,335 controls).

88

### 89 **Non-imaging features**

#### 90 **Clinical Outcomes**

91 Suicidal ideation and attempts were assessed from the computerized version of Kiddie  
92 Schedule for Affective Disorders and Schizophrenia (KSADS-COMP) reported by children or  
93 caregivers <sup>9</sup>. Validity of the computerized version of KSADS has been shown elsewhere<sup>9</sup>.  
94 Suicidal ideation was constructed to measure both passive suicidal ideation and active suicidal  
95 ideation<sup>10</sup>. Among the reports from children and parents, we used ones reporting more severe  
96 symptoms. In this study, we used suicide ideation as the main outcome and suicide attempt  
97 as the secondary target, given the data availability (fewer numbers of participants with suicide

98 attempts than ones with suicide ideation) and the consideration that suicide ideation precedes  
99 suicide attempt.

100

## 101 **Psychosocial features**

102 To estimate the feasibility of a brain-based prediction model, we constructed a  
103 psychosocial model as a benchmark model. The benchmark model consisted of demographic,  
104 psychological health, mental health, cognition, and environmental variables, which reported  
105 associations with suicidality in the literature.

106 Sociodemographic variables we considered were age, sex, race, highest parental  
107 education, family income, and parental marriage status. Physical health variables included  
108 anthropometric variables (height, weight, BMI, and brain volume) and sleep function assessed  
109 by Sleep Disturbances Scale for Children <sup>11</sup>. For mental health, we measured dimensional  
110 psychopathology (the Child Behavior Checklist <sup>12</sup>), impulsivity (UPPS-P <sup>13</sup>), mania symptoms  
111 (Parent General Behavior Inventory<sup>14</sup>), psychosis (ABCD prodromal psychosis scales <sup>15</sup>), and  
112 behavioral inhibition/approach system (PhenX modified version <sup>16</sup>). Cognitive ability was  
113 measured using NIH toolbox <sup>17</sup>. Environmental variables contained the measures of family  
114 conflict, early life stress (ELS), and friendship. Family conflict consisted of nine measures,  
115 which were assessed by ABCD Youth Family Environment Scale-Family Conflict Subscale  
116 Modified from PhenX. The ELS measures were composite variables based on child exposure  
117 domains in the ABCD study including household challenges, neglect, and abuse as main  
118 categories. Subcategories of ELS data contained parental separation or divorce, criminal  
119 household member, household substance abuse, mental illness in household, mother treated  
120 violently in household challenges, emotional neglect, physical neglect in neglect, physical  
121 abuse, and sexual abuse in abuse. The items of each subscale were derived from various  
122 instruments rated by children themselves or parents: ABCD Youth Family Environment Scale-  
123 Family Conflict Subscale Modified from PhenX, ABCD Diagnostic Interview for DSM-5

124 Traumatic Events, ABCD Family History Assessment, ABCD Parent Demographic Survey,  
125 ABCD Children's Report of Parental Behavioral Inventory, and ABCD Parental Monitoring  
126 Survey. We assigned 0 to those who have never had ELS and 1 to those who have at least  
127 one type. For three main categories, a child has 1 if at least one subcategory is 1. Missing  
128 values were imputed with Bayesian approach and then z-normalization was performed.

129

### 130 **Brain imaging analysis**

131 Brain imaging included in this study are as follows: structural MRI (sMRI), diffusion  
132 MRI (dMRI), resting-state functional MRI (rs-fMRI), and task-based functional MRI. For task-  
133 based functional MRI, participants performed three types of tasks including stop signal task  
134 (SST), the emotional version of N-back (N-back), and the monetary incentive delay task (MID).

135 MRI scanning was performed using a 3T scanner (Siemens Prisma, General Electric  
136 (GE) 750 and Philips). Image processing and quality assessment for the brain imaging  
137 datasets were performed at the ABCD Data Analysis and Informatics Center (DAIC). The  
138 ABCD MRI quality assessment consists of three parts: protocol compliance checking,  
139 automated quality metrics, manual review of data quality <sup>18</sup>. Firstly, protocol compliance  
140 checking examined whether key imaging parameters matched expected values of a given  
141 scanner, such as voxel size or repetition time. Secondly, quality control metrics were obtained  
142 for sMRI and fMRI. Mean motion and the number of slices and frames affected by slice dropout  
143 by head motion were controlled. Thirdly, the data quality was manually assessed by trained  
144 investigators as binary (0 = reject and 1 = accept) considering the image quality and the  
145 severity of the artifact (motion, intensity inhomogeneity, white matter underestimation, pial  
146 overestimation, magnetic susceptibility artifact). Images that failed to pass the quality  
147 assessment were excluded from the analysis.

148 We acquired multi-shell diffusion MRI from an ABCD study using the following protocol  
149 <sup>19</sup>. The ABCD Data Analysis and Informatics Center (DAIC) preprocessed diffusion MRI  
150 including distortion and motion correction. B0 distortion and gradient nonlinearity distortion  
151 were corrected <sup>20,21</sup>. We used individualized connectome data to estimate brain imaging  
152 phenotypes. Using MRtrix3, we preprocessed diffusion MRI (dMRI), estimated whole-brain  
153 white matter tracts, and generated an individualized connectome <sup>22</sup>. To estimate connectivity,  
154 we used streamline counts which represent the fiber connection strength associated with fiber  
155 integrity <sup>23,24</sup>. After decreasing the noise, we performed bias correction with the N4 algorithm  
156 of the Advanced Normalization Tools (ANTs) pipeline <sup>25</sup>. Of the target 20 million streamline  
157 counts, we filtered out preliminary tractograms with spherical-deconvolution for a 2:1 ratio.  
158 Finally, we generated an 84 x 84 whole-brain connectome matrix for each participant with 10  
159 million streamline counts using T1-based parcellation and segmentation from FreeSurfer. All  
160 the computation was carried out by supercomputers at the Argonne Leadership Computing  
161 Facility Theta and Texas Advanced Computing Center Stampede 2.

162 For resting-state functional MRI acquisition, participants completed four 5-minutes  
163 resting-state blood oxygen level-dependent scans, with their eyes open and fixated on a  
164 crosshair. Participants were also scanned during cognitive tasks. Resting-state functional MRI  
165 and task-based functional MRI data were processed and analyzed according to standardized  
166 ABCD protocols <sup>19</sup>. Because of post-processing problems on resting-state and task-based  
167 functional MRI data collected on the Philips scanners, all data from the Philips scanner were  
168 removed from the current analysis following the ABCD data analysis center's advice. For  
169 functional brain features, we used functional connectivity measures from resting-state fMRI  
170 and pairwise correlation coefficients between each region of interest (ROI) from task-based  
171 fMRI. The pairwise correlations were examined for ROIs within functionally defined  
172 parcellations (i.e., Gordon networks) and subcortical ROIs, and applied Fisher's  $r$  to  $z$ -  
173 transformation.

174

## 175           **Deep Neural Network**

176           Firstly, we split the data into discovery and replication sets. Within the discovery set,  
177 we trained, optimized, and validated models with stratified 5 fold cross validation. Secondly,  
178 we tested the generalizability of the optimized models on the balanced (down-sampled)  
179 replication set and then measured model performance with sensitivity, specificity, accuracy,  
180 area under the receiver operating characteristic curve (ROC-AUC), and area under the  
181 precision recall curve (AUPRC). These metrics were estimated using the pROC package v.  
182 1.16.2 in the R programming language and the sklearn package for average precision scores.

183           The benchmark model contained existing non-imaging variables about suicidality.  
184 These variables were also included in all neuroimaging models, since one of our research  
185 goals was to test whether neuroimaging data would be useful for suicide prediction.

186           For multimodal interpretable neuroimaging models for identifying youth suicidality, we  
187 used TabNet and further implemented stacking ensemble, GAN-based data augmentation,  
188 and dimension reduction methods. TabNet has been developed for tabular data enabling  
189 rigorous end-to-end deep learning with built-in interpretability <sup>26</sup>. This neural network is based  
190 on a sequential attention mechanism that gently selects features to infer at each decision step  
191 and then accumulates processed information to make final prediction decisions. By using  
192 sequential attention mechanisms, selecting sparse features, the model could learn efficiently  
193 at each decision-making stage. Therefore, the model with fully related variables shows high  
194 performance by taking advantage of related variables. This sparsity could allow for more  
195 interpretable decision-making through visualization of variable selection masks <sup>26</sup>. In this study,  
196 given the large feature space of the multimodal brain imaging data, TabNet would enable  
197 effective learning of latent representations of the complex data as well as interpretation of the  
198 models. Running a single TabNet experiment took around 18 hours on three V100 GPU cards.  
199 Hyper-parameter tuning was done by grid search. We changed the width of the attention  
200 embedding for each mask, coefficient for feature reuse in the masks, number of steps,

201 learning rate and weight decay. Thus, we used 32-dimension hyper-parameter spaces and  
202 found the best hyper-parameter dimension for each dataset.

203

## 204 **Stacking Ensemble Modeling**

205 Stacking ensemble algorithm, widely used ensemble methods along with voting and  
206 bagging, is a two-level classification consisting of base classifier level and meta-classifier level  
207 <sup>27</sup>. Previous studies showed that a multimodal stacked ensemble algorithm yielded better  
208 representation than single modal algorithms <sup>28,29</sup>. Therefore, we aimed to test the effects of  
209 stacking ensembles on multimodal neuroimaging data, and whether stacking ensemble  
210 methods take advantage of learning higher-level feature representation.

211 We generated stacking ensemble models whose output types of base learners are  
212 continuous probability values. Trained models of single neuroimaging data with TabNet are  
213 base learners. Train data and test data used at the meta-classifier level were concatenated  
214 with predicted results from cross-validation and testing in base learners. Logistic regression,  
215 xgboost, and random forest were used as meta-learners. The best results from the three meta-  
216 learners were reported.

217

## 218 **Data Augmentation**

219 For imbalance between case and controls in suicide prediction that might constrain  
220 representation learning, we implemented GAN-based data augmentation approaches through  
221 conditional tabular GAN <sup>30</sup>. Given the fact that youth suicidal ideation and attempts are rare  
222 events at the population level, we observed a highly imbalanced distribution between youth at  
223 risk for suicidality. Thus, augmented suicidality samples with synthesized data. We generated  
224 as many as samples until generated samples showed acceptable CTGAN metrics <sup>30</sup>:

225 logistic\_detection (Logistic Regression classifier to detect whether each row is real or synthetic,  
226 the returned score is 1 - ROC-AUC score obtained by the classifier): 0.99,  
227 svc\_detection(Support Vector Classifier to detect whether each row is real or synthetic): 0.92  
228 in rs-fMRI + sMRI + dMRI dataset and logistic\_detection: 0.99, svc\_detection: 0.99 in rs-fMRI  
229 + SST fMRI + N-back fMRI + MID fMRI dataset. As a result, the augmented discovery set was  
230 less imbalanced with a ratio of 1: 2.5.

231

### 232 **Dimension reduction**

233 We utilized TabNet and principal component analysis (PCA) to reduce dimensionality  
234 by selecting important features for modeling. For feature selection, we chose the top 50  
235 features (in TabNet) or components (in PCA) in each neuroimaging modality estimated in  
236 validation sets. This number was based on our observation that the rate of the increase in  
237 explainability slowed for more than 50 features (**Supplementary Figure 1**). For PCA, the full  
238 Singular Value Decomposition method was used <sup>31</sup>.

## 239 Results

### 240 Demographics

241 We used data from the ABCD study, a nationwide multisite prospective, longitudinal  
242 study. The enrolled samples consisted of 9 and 10-year-old children in the US across 21 sites.  
243 Total participants used in this analysis included 837 children with suicidality (i.e., Suicidal  
244 ideation or Suicidal attempt) and 5,335 controls (**Table 1**).

245

### 246 Identification of children with suicidal ideation using neuroimaging data

247 Our neuroimaging models for classification of suicidal ideation showed varied  
248 performances ranging from test ROC-AUCs of 48.26 to 61.22 (AURPCs: 47.85—60.06; **Table**  
249 **2**). Among the models trained on neuroimaging features only, the structural MRI, the diffusion  
250 MRI and the resting-state fMRI models (ROC-AUCs: 61.22—57.18, AURPCs: 52.74—60.06)  
251 provided higher performances than task fMRI models (ROC-AUCs: 48.26—53.42, AURPCs:  
252 47.85—50.87), which exceeded at chance level. All the neuroimaging models fell short of the  
253 classification performance of the psychosocial model, which yielded a moderate accuracy in  
254 classifying children with suicidal ideation and controls (ROC-AUC = 74.16, AUPRC: 70.18).

255

256

### 257 Combining psychosocial and imaging-based data showed improvements in 258 identifying children with suicidality.

259 When combining behavioral and brain imaging-derived phenotypes, models showed  
260 moderately accurate performance in classifying children with suicidal ideation, ranging from

261 ROC-AUC 69.54% to ROC-AUC 74.16% (AUPRC: 64.79—67.85; **Table 2**). Moreover, to  
262 address problems brought from the large feature space of multimodal neuroimaging data, we  
263 implemented dimension reduction and data augmentation strategies to further optimize the  
264 suicide prediction models. We found that deep neural net-based feature selection led to  
265 marginal improvement of ROC-AUC in the combined models of structural MRI, diffusion MRI,  
266 SST fMRI, and MID fMRI. Of note, the diffusion MRI model outperformed the benchmark  
267 model by a small margin (diffusion MRI: 74.82 ROC-AUC, 70 AUPRC).

268

### 269 **Integration of multimodal neuroimaging data**

270 We further investigated whether fusing psychosocial and multimodal neuroimaging  
271 data could improve the identification of suicidal ideation. While most multimodal neuroimaging  
272 models failed to show better classification than the benchmark model, two models (i.e., dMRI  
273 + rs-fMRI, rs-fMRI + sMRI + dMRI) showed comparable ROC-AUCs to that of the benchmark  
274 model (**Table 3**). These models were based on feature selection and ensemble methods.

275 Also, the combined model of sMRI and dMRI, which represents brain morphology and  
276 structural connectivity of white matter, offered higher ROC-AUC compared with the single  
277 modal performances of sMRI and dMRI, respectively. We also found that integrating functional  
278 MRIs slightly exceeded the performance of each single modality model: e.g., rs-fMRI + SST  
279 fMRI: 73.58 ROC-AUC, rs-fMRI + N-back fMRI: 73.82 ROC-AUC.

280 Compared with the same multimodal models trained on original features, the feature  
281 selected models provided slightly higher performances. In ensemble models, while the  
282 connectivity models (i.e., sMRI, dMRI, rs-fMRI) showed slight improvements in test ROC-  
283 AUCs, the models trained on task fMRI-derived activation estimates showed a sharp decrease  
284 to 53.94—56.71 ROC-AUCs.

285

## 286 **Model Interpretation**

287           Across modalities, the feature importance plots of our models included brain derived  
288 features related to anterior cingulate cortex, temporal gyrus, and precentral gyrus (**Figure 1**).  
289 Common psychological features were observed including Internalizing-externalizing  
290 comorbidity, Prodromal psychosis, Anxiety, Depression, and Family conflict. These  
291 multimodal features showed patterns in predicting the risk for suicidal ideation across  
292 modalities: top 2~17% features accounted for 90% performances. These important features  
293 consisted of small numbers of psychological features (9~17%) and large amounts of  
294 neuroimaging derived features (83~90%). Complete feature importance details are in  
295 **Supplementary Figure 2.**

296

## 297 Discussion

298 We tested deep neural networks trained on the largest youth brain multimodal MRI  
299 data, as well as parent-reported psychosocial questionnaires, to predict youth with suicidal  
300 thoughts. Our deep neural networks showed both feasibility and limitations of the brain-based  
301 risk prediction of youth suicidality. Throughout our systematic model comparison, the one  
302 trained on white matter connectivity and psychological data performed the best. Models  
303 trained on multimodal brain imaging-derived data alone, including white matter connectivity,  
304 morphometry, functional connectivity, and task reactivity, showed above-chance performance  
305 yet were poorer compared with the baseline psychological model. Model interpretation showed  
306 the cortical regions and connections of which structural or functional metrics contributed to the  
307 prediction of youth suicidality, including the inferior frontal, temporal, precentral gyri, insula,  
308 and anterior cingulate cortex. These results from large, multi-site, epidemiological samples  
309 show the feasibility of the data-driven computational learning approach to multimodal brain  
310 MRI for prediction, as well as scientific discovery of youth suicidality.

311 The brain alone models showed statistically meaningful classification performance with  
312 the maximum ROC-AUC of 61.22 in resting-state fMRI-functional connectivity and similarly in  
313 structural and diffusion MRI-derived estimates. Prior studies with small sample sizes (e.g., N  
314 < 160) in adults report moderate accuracy in predicting suicidal ideation or attempts based on  
315 structural and functional brain imaging (with ROC-AUC ranging from 0.72 to 0.94; some results  
316 from only cross-validation but not from held-out test set)<sup>6,7,32,33</sup>. Conversely, literature in  
317 children has been extremely rare. To our knowledge, this is the first study reporting the  
318 machine learning application to neuroimaging data to identify youth with suicidality.

319 Our neural networks permit delineating the brain correlates of youth suicidality. Our  
320 integrative models combining the psychosocial and white matter connectivity showed a slight  
321 increase in model performance (with a 1% ROC-AUC) compared with the baseline  
322 psychosocial model. Important features in this model include white matter connectivity,

323 morphometry, and functional connectivity within the distributed brain network, primarily the  
324 neocortex, including the inferior frontal gyrus, insula, and anterior cingulate cortex. The inferior  
325 frontal gyrus plays a role in emotional regulation, sustained attention, and language  
326 processing<sup>34</sup>, of which abnormalities were associated with suicidality in adolescents<sup>35</sup>. The  
327 insula and anterior cingulate cortex, as part of the salience network, are involved in the  
328 detection and integration of emotional and sensory stimuli<sup>36</sup>. These features selected by the  
329 deep neural network with the sequential attention mechanism, are largely overlapped with  
330 those selected in the linear mass-univariate analysis in a prior study<sup>37</sup> (note that this prior study  
331 did not include diffusion MRI). Despite neither the mass-univariate nor machine learning  
332 approach can present the causal brain circuitry underlying suicide, the brain circuit correlates  
333 found in this study may help future research in youth suicidality.

334         Considering the previous univariate statistical analysis of the same data reporting the  
335 low classification accuracy (with area under precision-recall less than 0.10) for youth suicidality  
336 using brain imaging (cf. without diffusion data)<sup>37</sup>, our results of the maximum ROC-AUC of  
337 0.75 (area under precision-recall of 0.70) in held-out test samples show the importance of  
338 nonlinear multimodal modeling with machine learning in individualized prediction. Then, a  
339 more highly parameterized, end-to-end learning model trained on 3D and 4D brain MRI would  
340 improve accuracy to the level of practicality. Despite that a recent study shows a poorer  
341 scalability of the end-to-end deep learning models than linear models with the size of 10,000  
342 samples<sup>38</sup>, which was based on the tasks to predict common biological phenotypes (e.g., age  
343 and sex), we believe it is necessary to test the very scalability of this approach in the task of  
344 youth suicidality prediction. Moreover, even if the brain imaging itself contributes to the  
345 prediction with a limited degree, integrating the multi-modal data, not limited to the brain  
346 imaging, but extending to genetics, microbiome, life-log data, SNS and speech data may help  
347 us build a better predictive model with the practical utility in clinical or school settings.

348         Our deep neural networks trained on psychological and multimodal neuroimaging data  
349 may reflect the interplay between psychological variables and brain circuits related to risk for

350 youth suicidality. This is based on our observations of model interpretation across modalities:  
351 About 20% of features accounted for more than a 90% variance. Of those, besides several  
352 psychological features (e.g., internalizing symptoms) the multimodal brain phenotypes  
353 constitute the majority. Although the performance boost owing to the brain data was limited  
354 with up to a 1% ROC-AUC increase, we find this observation may reflect the interaction  
355 between the internalizing symptoms and the distributed brain system contributing to youth  
356 suicidality.

357 Our models include common psychosocial features as important attributes (e.g.,  
358 internalizing and depressive behaviors, prodromal psychosis, and family conflict). This result  
359 is consistent with previous suicidality literature and recent findings from the ABCD study <sup>2,10,39</sup>.

360 We tested two different methods of dimensionality reduction to overcome the sample  
361 complexity problem, i.e., the large feature space compared with the sample size. Overall,  
362 performance improvements were trivial. TabNet-based feature selection significantly improved  
363 performance compared to the models trained on original features, while PCA showed no  
364 improvements. Since TabNet's sequential attention mechanism accounts for the nonlinearity  
365 of the relationships among the features, which PCA cannot do so, this result implies the  
366 importance of non-linear modeling of the brain data in predicting suicidality in children.

367 Our stacking ensemble approach showed no benefits of integrating multi-modal brain  
368 imaging data. We believe that the stacking approach may have failed to account for  
369 complementary characteristics across the modalities. For better multi-modal integration, a  
370 principled approach that can utilize multitude representations as well as the brain network  
371 organization might be tested in the future. A recent breakthrough in computational chemistry  
372 may be a good example. A graph neural network accurately predicts protein folding structures  
373 and interactions by learning rich representations about proteins from multimodal and  
374 multidimensional data<sup>40</sup>.

375           Likewise, in our experiment, performance increases by GAN-based data augmentation  
376 were not meaningful in the replication set (while it significantly improved performance in the  
377 validation set). This may be due to different distributions between the discovery and replication  
378 set<sup>41</sup>. In the future, since the benefits of the dimensionality reduction were observed in this  
379 study (e.g., TabNet’s sequential attention mechanism), it will be interesting to test the data  
380 augmentation method in reduced numbers of the brain features.

381           There are some limitations to be considered in future studies. Firstly, suicidality (which  
382 includes suicidal ideation and attempt) does not always lead to suicidal commitment <sup>42</sup>. This  
383 might result from the difficulty not only of collecting data on who committed suicide but also of  
384 obtaining sufficient samples of suicide attempts from prepubertal children. Secondly, this study  
385 used a cross-sectional design. This limits us to testing the causal relationship between brain  
386 data and suicidality, or predictability of future outcomes. Given that the brain organizations of  
387 prepubertal children mature throughout adolescence, future research should test prospective  
388 predictions of suicidal risk using longitudinal data.

389           In sum, this study demonstrates the potential utility of a deep neural network approach  
390 using both psychosocial variables and neuroimaging to identify prepubertal children at risk for  
391 suicide in large, representative, and multi-site samples.

## 392           **Acknowledgments**

393           This work was supported by the New Faculty Startup Fund from Seoul National University (Cha);  
394 the BK21 FOUR Program (5199990314123) through the National Research Foundation of Korea (Cha  
395 and Ahn); National IT Promotion Agency GPU award (Cha); Intel PRTI award (Cha).

396

397 **Data and code availability**

398 The ABCD data can be accessed via the NIMH Data Archive (<https://nda.nih.gov/>). Our

399 codes used in this study are freely accessible: for the Tabnet implementation

400 (<https://colab.research.google.com/drive/1y5l89AxfGYAIJmW2jnYk42OOIDfP8Zz?usp=share>

401 [ing](#)) and for the ensemble modeling

402 ([https://colab.research.google.com/drive/1IR1Y5BBEuGtxQfDDYZ2RL9EtL\\_h\\_Jxf?usp=sharing](https://colab.research.google.com/drive/1IR1Y5BBEuGtxQfDDYZ2RL9EtL_h_Jxf?usp=sharing))

## 403 **References**

- 404 1. Beautrais, A. L. Suicide and serious suicide attempts in youth: a multiple-group  
405 comparison study. *Am. J. Psychiatry* 160, 1093–1099 (2003).
- 406 2. DeVille, D. C. et al. Prevalence and Family-Related Factors Associated With Suicidal  
407 Ideation, Suicide Attempts, and Self-injury in Children Aged 9 to 10 Years. *JAMA Netw*  
408 *Open* 3, e1920956 (2020).
- 409 3. Tsypes, A., Owens, M. & Gibb, B. E. Blunted Neural Reward Responsiveness in Children  
410 with Recent Suicidal Ideation. *Clin. Psychol. Sci.* 7, 958–968 (2019).
- 411 4. Huber, R. S., Sheth, C., Renshaw, P. F., Yurgelun-Todd, D. A. & McGlade, E. C. Suicide  
412 Ideation and Neurocognition Among 9- and 10-Year Old Children in the Adolescent  
413 Brain Cognitive Development (ABCD) Study. *Arch. Suicide Res.* 1–15 (2020).
- 414 5. Chen, K., Azeez, A., Chen, D. Y. & Biswal, B. B. Resting-State Functional Connectivity:  
415 Signal Origins and Analytic Methods. *Neuroimaging Clinics of North America* vol. 30 15–  
416 23 (2020).
- 417 6. Gosnell, S. N., Fowler, J. C. & Salas, R. Classifying suicidal behavior with resting-state  
418 functional connectivity and structural neuroimaging. *Acta Psychiatrica Scandinavica* vol.  
419 140 20–29 (2019).
- 420 7. Just, M. A. et al. Machine learning of neural representations of suicide and emotion  
421 concepts identifies suicidal youth. *Nature Human Behaviour* vol. 1 911–919 (2017).
- 422 8. Calhoun, V. D. & Sui, J. Multimodal Fusion of Brain Imaging Data: A Key to Finding the  
423 Missing Link(s) in Complex Mental Illness. *Biological Psychiatry: Cognitive*  
424 *Neuroscience and Neuroimaging* vol. 1 230–244 (2016).
- 425 9. Townsend, L. et al. Development of Three Web-Based Computerized Versions of the  
426 Kiddie Schedule for Affective Disorders and Schizophrenia Child Psychiatric Diagnostic  
427 Interview: Preliminary Validity Data. *J. Am. Acad. Child Adolesc. Psychiatry* 59, 309–  
428 325 (2020).
- 429 10. Harman, G. et al. Prediction of suicidal ideation and attempt in 9 and 10 year-old

- 430 children using transdiagnostic risk features. *PLoS One* 16, e0252114 (2021).
- 431 11. Bruni, O. et al. The Sleep Disturbance Scale for Children (SDSC). Construction and  
432 validation of an instrument to evaluate sleep disturbances in childhood and  
433 adolescence. *J. Sleep Res.* 5, 251–261 (1996).
- 434 12. Watts, A. L., Smith, G. T., Barch, D. M. & Sher, K. J. Factor structure, measurement and  
435 structural invariance, and external validity of an abbreviated youth version of the UPPS-  
436 P Impulsive Behavior Scale. *Psychol. Assess.* 32, 336–347 (2020).
- 437 13. Karcher, N. R. et al. Assessment of the Prodromal Questionnaire-Brief Child Version for  
438 Measurement of Self-reported Psychoticlike Experiences in Childhood. *JAMA*  
439 *Psychiatry* 75, 853–861 (2018).
- 440 14. Pagliaccio, D. et al. Revising the BIS/BAS Scale to study development: Measurement  
441 invariance and normative effects of age and sex from childhood through adulthood.  
442 *Psychol. Assess.* 28, 429–442 (2016).
- 443 15. Akshoomoff, N. et al. VIII. NIH Toolbox Cognition Battery (CB): composite scores of  
444 crystallized, fluid, and overall cognition. *Monogr. Soc. Res. Child Dev.* 78, 119–132  
445 (2013).
- 446 16. Hagler, D. J., Jr et al. Automated white-matter tractography using a probabilistic  
447 diffusion tensor atlas: Application to temporal lobe epilepsy. *Hum. Brain Mapp.* 30,  
448 1535–1547 (2009).
- 449 17. Hagler, D. J., Jr et al. Image processing and analysis methods for the Adolescent Brain  
450 Cognitive Development Study. *Neuroimage* 202, 116091 (2019).
- 451 18. Holland, D., Kuperman, J. M. & Dale, A. M. Efficient correction of inhomogeneous static  
452 magnetic field-induced distortion in Echo Planar Imaging. *Neuroimage* 50, 175–183  
453 (2010).
- 454 19. Wells, W. M., 3rd, Viola, P., Atsumi, H., Nakajima, S. & Kikinis, R. Multi-modal volume  
455 registration by maximization of mutual information. *Med. Image Anal.* 1, 35–51 (1996).
- 456 20. Tournier, J.-D. et al. MRtrix3: A fast, flexible and open software framework for medical  
457 image processing and visualisation. *Neuroimage* 202, 116137 (2019).

- 458 21. Cha, J. et al. Abnormal reward circuitry in anorexia nervosa: A longitudinal, multimodal  
459 MRI study. *Hum. Brain Mapp.* 37, 3835–3846 (2016).
- 460 22. Cha, J. et al. Neural Correlates of Aggression in Medication-Naive Children with ADHD:  
461 Multivariate Analysis of Morphometry and Tractography. *Neuropsychopharmacology* 40,  
462 1717–1725 (2015).
- 463 23. Tustison, N. J. et al. N4ITK: improved N3 bias correction. *IEEE Trans. Med. Imaging* 29,  
464 1310–1320 (2010).
- 465 24. Shunmugapriya, P. & Kanmani, S. Optimization of stacking ensemble configurations  
466 through Artificial Bee Colony algorithm. *Swarm and Evolutionary Computation* vol. 12  
467 24–32 (2013).
- 468 25. Yang, Y. et al. Classification of Parkinson’s disease based on multi-modal features and  
469 stacking ensemble learning. *J. Neurosci. Methods* 350, 109019 (2021).
- 470 26. Chaurasia, V. & Pal, S. Stacking-Based Ensemble Framework and Feature Selection  
471 Technique for the Detection of Breast Cancer. *SN Computer Science* vol. 2 (2021).
- 472 27. Lei Xu (S. Synthesizing Tabular Data Using Conditional GAN. (2020).
- 473 28. Halko, N., Martinsson, P. G. & Tropp, J. A. Finding Structure with Randomness:  
474 Probabilistic Algorithms for Constructing Approximate Matrix Decompositions. *SIAM*  
475 *Review* vol. 53 217–288 (2011).
- 476 29. Hong, S. et al. Identification of suicidality in adolescent major depressive disorder  
477 patients using sMRI: A machine learning approach. *J. Affect. Disord.* 280, 72–76 (2021).
- 478 30. Weng, J.-C. et al. An Autoencoder and Machine Learning Model to Predict Suicidal  
479 Ideation with Brain Structural Imaging. *J. Clin. Med. Res.* 9, (2020).
- 480 31. Greenlee, J. D. W. et al. Functional connections within the human inferior frontal gyrus.  
481 *The Journal of Comparative Neurology* vol. 503 550–559 (2007).
- 482 32. Ordaz, S. J., Goyer, M. S., Ho, T. C., Singh, M. K. & Gotlib, I. H. Network basis of  
483 suicidal ideation in depressed adolescents. *J. Affect. Disord.* 226, 92–99 (2018).
- 484 33. White, T. P., Joseph, V., Francis, S. T. & Liddle, P. F. Aberrant salience network  
485 (bilateral insula and anterior cingulate cortex) connectivity during information processing

- 486 in schizophrenia. *Schizophrenia Research* vol. 123 105–115 (2010).
- 487 34. Vidal-Ribas, P. et al. Multimodal neuroimaging and suicidality in a US population-based  
488 sample of school-aged children. doi:10.1101/19013193.
- 489 35. Schulz, M.-A. et al. Different scaling of linear models and deep learning in UKBiobank  
490 brain images versus machine-learning datasets. *Nat. Commun.* 11, 4238 (2020).
- 491 36. Janiri, D. et al. Risk and protective factors for childhood suicidality: a US population-  
492 based study. *Lancet Psychiatry* 7, 317–326 (2020).
- 493 37. Vidal-Ribas, P., Janiri, D., Doucet, G. E., Pornpattananangkul, N., Nielson, D. M., Frangou, S., &  
494 Stringaris, A. (2020). Multimodal neuroimaging and suicidality in a US population-based sample  
495 of school-aged children. *medRxiv*, 19013193.
- 496 38. Jain, V. & Chatterjee, J. M. *Machine Learning with Health Care Perspective: Machine*  
497 *Learning and Healthcare*. (Springer Nature, 2020).
- 498 39. Fridley, B. L. Data augmentation for the handling of censored spatial data.  
499 doi:10.31274/rtd-180813-12076.
- 500 40. Chen, J., Chun, D., Patel, M., Chiang, E. & James, J. The validity of synthetic clinical  
501 data: a validation study of a leading synthetic data generator (Synthea) using clinical  
502 quality measures. *BMC Med. Inform. Decis. Mak.* 19, 44 (2019).
- 503 41. Baur, C., Albarqouni, S. & Navab, N. Generating Highly Realistic Images of Skin  
504 Lesions with GANs. *Lecture Notes in Computer Science* 260–267 (2018)  
505 doi:10.1007/978-3-030-01201-4\_28.
- 506 42. Sigfusdottir, I. D., Asgeirsdottir, B. B., Gudjonsson, G. H. & Sigurdsson, J. F. Suicidal  
507 ideations and attempts among adolescents subjected to childhood sexual abuse and  
508 family conflict/violence: the mediating role of anger and depressed mood. *J. Adolesc.*  
509 36, 1227–1236 (2013).

510 **Tables**

511 **Table 1. Sociodemographics of the study participants (n=6,172).**

	Controls		SI		SA		Statistics	p-value
N	5335		782		55			
Suicidal ideation					51			
Age	119 ± 7.4		119 ± 7.42		121 ± 6.08		F = 2.295	0.101
Sex								
Male	2704	50.68	465	59.46	36	65.45	Chisq = 25.123	p<.001
Female	2631	49.32	317	40.54	19	34.55		
Race / Ethnicity								
White	2994	56.12	426	54.48	20	36.36	Chisq = 32.56	p<.001
Black	482	9.03	69	8.82	13	23.64		
Hispanic	1183	22.17	157	20.08	18	32.73		
Asian	120	2.25	20	2.56	1	1.82		
Other	551	10.33	110	14.07	3	5.45		
Parents married	3858	72.31	517	66.11	26	47.27	Chisq = 28.489	p<.001
Income level	7.42 ± 2.26		7.22 ± 2.29		5.66 ± 2.6		F = 18.551	p<.05

512

513 **Table 2. Classification performances of psychosocial, imaging-based, and combined**  
 514 **deep neural networks identifying suicidal ideation.** Deep neural network (TabNet) and  
 515 additional methods for dimensionality reduction (feature selection, PCA) and data  
 516 augmentation (CTGAN) were tested.

Model	Replication set				
	ROC-AUC	AUPRC	Accuracy	Sensitivity	Specificity
<b>Psychosocial model</b>	74.16	70.18	70.66	72.78	68.55
<b>Structural MRI</b>					
Neuroimaging model	57.18	52.74	57.53	43.81	70.18
Combined model	71.44	67.95	67.82	84.18	51.57
Neural net based feature selected	72.55 †	69.05	69.72	75.32	64.15
PCA based dimension reduced	67.44	63.18	65.93	71.52	60.38
GAN based data augmented	69.74	65.08	67.51	78.48	56.60
<b>Diffusion MRI</b>					
Neuroimaging model	58.15	53.48	58.9	64.76	53.51
Combined model	69.54	64.79	66.88	74.68	59.12
Neural net based feature selected	<b>74.82 *</b>	70.06	72.24	75.95	68.55
PCA based dimension reduced	69.1	65.31	66.56	75.95	57.23
GAN based data augmented	68.74	64.09	65.93	73.42	58.49
<b>Resting state fMRI</b>					
Neuroimaging model	61.22	60.06	59.82	82.86	38.6
Combined model	73.74	67.58	70.34	86.07	54.71
Neural net based feature selected	73.43	70.86 *	69.72	72.78	66.67
PCA based dimension reduced	69.95	62.02	67.51	81.01	54.09
GAN based data augmented	71.26	66.92	67.51	81.65	53.46
<b>Stop signal task fMRI</b>					
Neuroimaging model	53.42	50.87	54.79	55.24	54.39
Combined model	71.37	67.6	67.51	65.79	69.11
Neural net based feature selected	72.52 <sup>†</sup>	68.41	67.93	62.28	73.17
PCA based dimension reduced	66.61	61.22	66.24	65.79	66.67
GAN based data augmented	70.24	65.05	66.24	71.05	61.79
<b>N-back task fMRI</b>					
Neuroimaging model	50.43	47.85	53.88	50.48	57.02
Combined model	72.69	66.73	70.04	81.58	59.35
Neural net based feature selected	72.09	68.71	68.78	75.44	62.60

PCA based dimension reduced	68.29	61.99	65.82	54.39	76.42
GAN based data augmented	68.78	62.29	66.67	85.09	49.59
<b>Monetary incentive delay task fMRI</b>					
Neuroimaging model	48.26	49.47	54.79	64.76	45.61
Combined model	71.22	66.19	65.82	65.79	65.85
Neural net based feature selected	72.28 <sup>†</sup>	68.89	70.04	71.93	68.29
PCA based dimension reduced	64.58	60.86	64.14	62.28	65.85
GAN based data augmented	68.23	63.39	66.67	73.68	60.16

517 Note: Combined models included imaging derived and psychosocial features. \* indicates  
518 higher performance than the benchmark result in TabNet and † indicates higher performances  
519 than TabNet results in the same dataset.

---

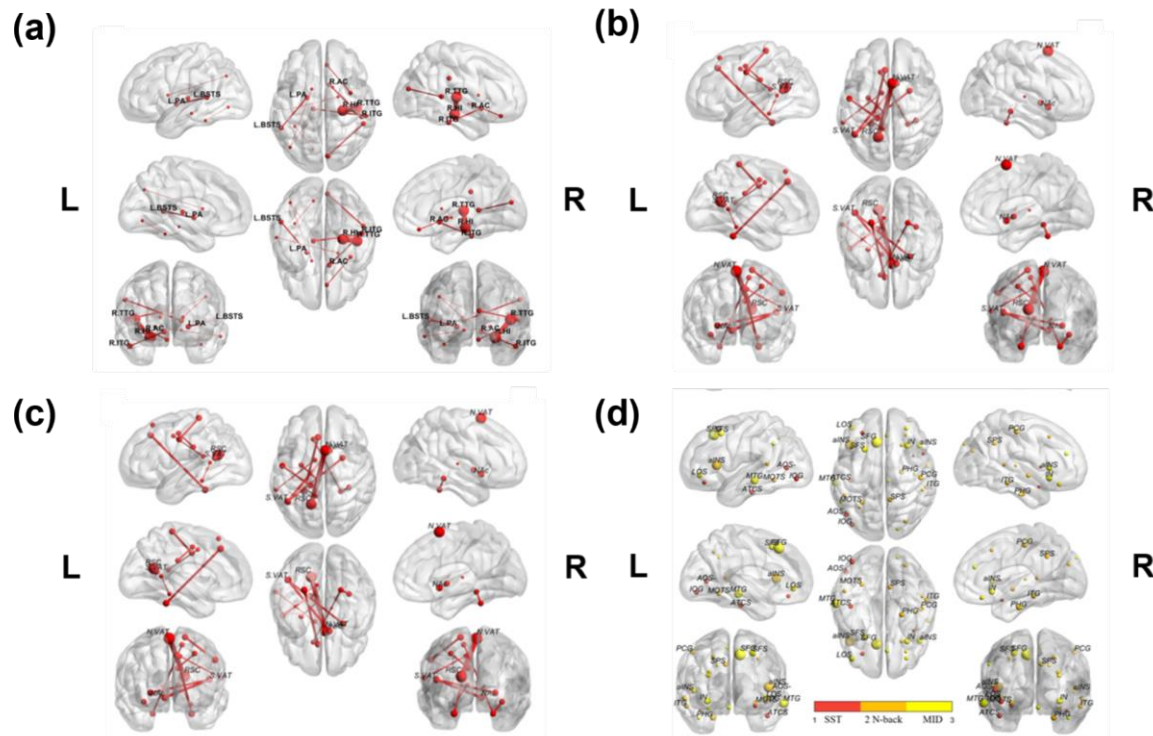
520

521

522 **Table 3.** Classification performances (ROC AUC) of psychosocial and multimodal  
523 neuroimaging data for identification of suicide ideation on balanced replication datasets.

	Model	TabNet	TabNet - Feature selection	Ensemble
Morphometry and connectivity	sMRI + dMRI	73.81 ‡	72.3	73.91 <sup>†</sup>
	sMRI + rs-fMRI	72.43	72.71 <sup>†</sup>	73.77 <sup>†</sup>
	dMRI + rs-fMRI	72.86	73.28	<b>74.7*</b>
	rs-fMRI + sMRI + dMRI	68.47	<b>74.43 *</b>	<b>74.41*</b>
Functional connectivity and activation	rs-fMRI + SST fMRI	73.58 ‡	72.23	54.97
	rs-fMRI + Nback fMRI	73.82 ‡	72.31	56.22
	SST fMRI + Nback fMRI	71	72.48 <sup>†</sup>	56.71
	SST fMRI + Nback fMRI + MID fMRI	71	72.74 <sup>†</sup>	53.94
	rs-fMRI + SST fMRI+ Nback fMRI + MID fMRI	70.43	69.91	56.51
All modalities	sMRI + dMRI + rs-fMRI + SST fMRI + Nback fMRI + MID fMRI	65.9	69.76 <sup>†</sup>	54.95

524 \* represents higher performances than the psychosocial model with ROC AUC of 74.16. † denotes  
525 higher performances than TabNet results in the same dataset. ‡ denotes higher performances than the  
526 combined model trained on single neuroimaging data.



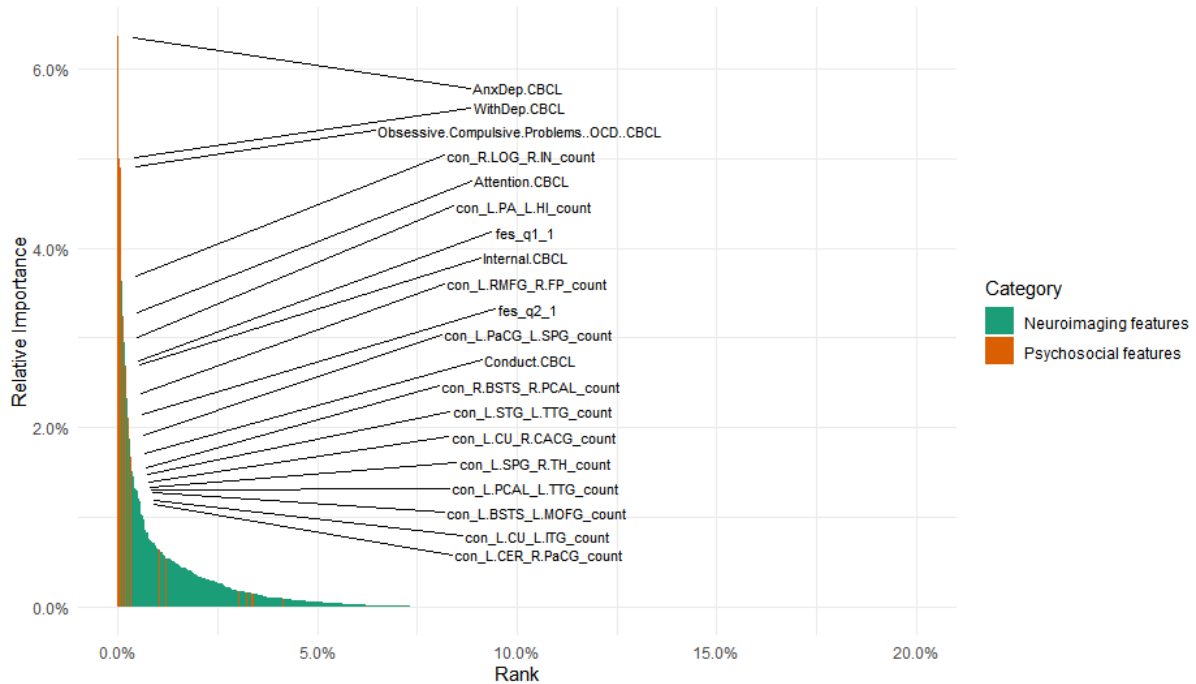
527

528 **Figure 1. Important neuroimaging features contributing to the identification of suicidal**  
 529 **ideation in combined models with selected features.** A. dMRI-derived White Matter  
 530 Connectivity. B. Structure MRI-Derived Morphometry. C. RS-FMRI-Derived Functional  
 531 Connectivity. D. Task FMRI-Derived Activation Estimates (Stop signal task, emotional N-  
 532 back task, monetary incentive delay task). The size of the node and edge represents the  
 533 relative importance.

534 **dMRI-derived White Matter Connectivity** L.BSTS: Left Banks of Superior Temporal Sulcus, L.PA: Left-Pallidum.  
 535 R.AC: Right-Accumbens-area, R.HI: Right-Hippocampus, R.ITG: gray matter of right inferior temporal gyrus,  
 536 R.TTG: gray matter of right transverse temporal gyrus./ **Structure MRI-Derived Morphometry** caudalMFG: caudal  
 537 middle frontal, frontal pole: frontal pole, fusiform-G: fusiform gyrus, Insula: superior segment of\_the circular sulcus  
 538 of the\_insula, lingual-gyrus: lingual-gyrus, occipital-pole: occipital pole, rostral-ACC: rostral anterior  
 539 cingulate, subcallosal-G: subcallosal gyrus/ **RS-FMRI-Derived Functional Connectivity** N.VAT: Network ventral  
 540 attention, NAc: nucleus accumbens, RSC: retrosplenial temporal cortex, S.VAT: Subcort ventral attention, / **Task**  
 541 **FMRI-Derived Activation Estimates** aINS: vertical ramus of the anterior segment of the lateral sulcus, aINS:  
 542 vertical ramus of the anterior segment of the lateral sulcus, AOS: anterior occipital sulcus and preoccipital notch,  
 543 ATCS: anterior transverse collateral sulcus, IN: superior segment of the circular sulcus of the insula, IOG: inferior  
 544 occipital gyrus and sulcus, LOS: lateral orbital sulcus, MTG: middle temporal gyrus, PCG: postcentral gyrus, PHG:

545 parahippocampal gyrus, SFG: superior frontal gyrus, SFS: superior frontal sulcus, SPS: subparietal sulcus

546 **Figure 2. Feature importance plot of diffusion MRI combined model.** Important 20  
 547 features are indicated. Top 5% features (N=180) exceed 95% of cumulative importance.  
 548



549  
 550 AnxDep.CBCL: Anxious/depressed behavior, Attention.CBCL: Attention problems, con\_R.LOG\_R.IN\_count:  
 551 connectivity between right lateral occipital gyrus and right insula, con\_L.PA\_L.HI\_count: connectivity between left  
 552 pallidum and left hippocampus, con\_L.RMFG\_R.FP\_count: connectivity between left rostral middle frontal gyrus  
 553 and right frontal pole, con\_L.PaCG\_L.SPG\_count: connectivity between left parahippocampal gyrus and right  
 554 subparietal gyrus, con\_R.BSTS\_R.PCAL\_count: connectivity between right bankssts and right pericalcarine,  
 555 con\_L.STG\_L.TTG\_count: connectivity between left superior temporal gyrus and left transverse temporal gyrus, ,  
 556 con\_L.CU\_R.CACG\_count: connectivity between left cuneus and right caudal anterior cingulate,  
 557 con\_L.SPG\_R.TH\_count: connectivity between left superior parietal gyrus and right thalamus,  
 558 con\_L.PCAL\_L.TTG\_count: connectivity between left pericalcarine and right transverse temporal gyrus,  
 559 con\_L.BSTS\_L.MOFG\_count: connectivity between left bankssts and right medial orbitofrontal gyrus,  
 560 con\_L.CU\_L.ITG\_count: connectivity between left cuneus and gray matter of left inferior temporal gyrus,  
 561 con\_L.CER\_R.PaCG\_count: connectivity between left Cerebellum-Cortex and right paracentral gyrus,  
 562 Conduct.CBCL: Conduct problems, conflict\_openly angry, fes\_q1\_1: Family\_frequent fights, fes\_q2\_1: Family,  
 563 Internal.CBCL: Internalizing behavior, Obsessive.Compulsive.Problems..OCD..CBCL: OCD problems,  
 564 WithDep.CBCL: Withdrawn/depressed behavior  
 565

566 **Identifying Prepubertal Children with Risk for Suicide Using Deep**  
567 **Neural Network Trained on Multimodal Brain Imaging-Derived**  
568 **Phenotypes**

569 **Bo-Gyeom Kim, Gun Ahn, Sooyoung Kim, Ka-Kyeong Kim, Hyeonjin Kim, Eunji Lee,**  
570 **Woo-Young Ahn, Jae-Won Kim, Jiook Cha**

571

572 **Supplementary Materials**

573 **Supplementary Table 1-4**

574 **Supplementary Figure 1-2**

575

576

577

578

579

580

581

582

583 **Supplementary Table 1.** Classification performances in predicting youth suicidality  
584 attempt. Deep neural networks (TabNet) and additional methods of dimensionality reduction  
585 and data augmentation were tested.

Model	TabNet	TabNet - Feature selection	TabNet - PCA	TabNet - CTGAN
Psychosocial	83.33 <sup>‡</sup>	69.44	-	69.44
Structural MRI	60.68	75 <sup>†</sup>	75 <sup>†</sup>	75 <sup>†</sup>
Diffusion MRI	72.22 <sup>‡</sup>	79.17 <sup>†</sup>	72.2	79.17 <sup>†</sup>
Resting state fMRI	80.56 <sup>‡</sup>	80.56	84.72 *	80.56
Stop signal task fMRI	78.1 <sup>‡</sup>	76.91	64.29	76.91
N-back task fMRI	69.05	78.57 <sup>†</sup>	76.19 <sup>†</sup>	78.57 <sup>†</sup>
Monetary incentive delay task fMRI	54.76	54.76	78.57	54.76

586 Note: All single modality models except psychosocial model included psychosocial by  
587 default. \* denotes higher performance than the benchmark result in TabNet and † denotes higher  
588 performances than TabNet results in the same dataset. ‡ denotes higher performances than the results  
589 in suicidality ideation using TabNet.

590

591 On the single modal neuroimaging data, the neural networks, TabNet showed a wider  
592 range of accurate performances in classifying children with suicidal attempts, ranging from  
593 ROC-AUC 54.76% to ROC-AUC 83.33%.

594 When we apply feature selection to TabNet, in structural and diffusion MRI, additional  
595 methods including feature selection, PCA and CTGAN showed higher performance than just  
596 TabNet model. Although there isn't any higher result than benchmark in both MRI data, we  
597 found that dimensionality reduction explains suicidality ideation and attempt better than the  
598 other ways.

599 **Supplementary Table 2.** Summed contribution of top 50 important features of the  
600 combined models to identify children at risk for suicidal ideation using TabNet.

<b>Model</b>	<b>Psychosocial variable</b>	<b>Neuroimaging variables</b>
Structural MRI	0.343	0.334
Diffusion MRI	0.296	<b>0.359</b>
Resting state fMRI	0.585	0.133
Stop signal task fMRI	0.382	0.343
N-back fMRI	0.435	0.245
Monetary incentive delay fMRI	0.456	0.252

601

602           **Supplementary Table 3.** Summed contribution of top 50 important features of suicidal  
603 attempt prediction models using TabNet

<b>Model</b>	<b>Psychosocial variable</b>	<b>Neuroimaging variables</b>
Structural MRI	0.218	0.307
Diffusion MRI	<b>0.329</b>	0.143
Resting state fMRI	0.129	0.411
Stop signal task fMRI	0.0966	0.453
N-back fMRI	0.105	0.396
Monetary incentive delay fMRI	0.0321	0.414

604    In the suicide attempt prediction task, we observed that most neuroimaging variables  
605 outweighed psychosocial variables in several neuroimaging models (structural MRI, resting-  
606 state fMRI, stop signal task fMRI, N-back task fMRI and monetary incentive delay task fMRI  
607 models). However, only diffusion MRI derived features outperformed psychosocial variables  
608 among the top 50 features.

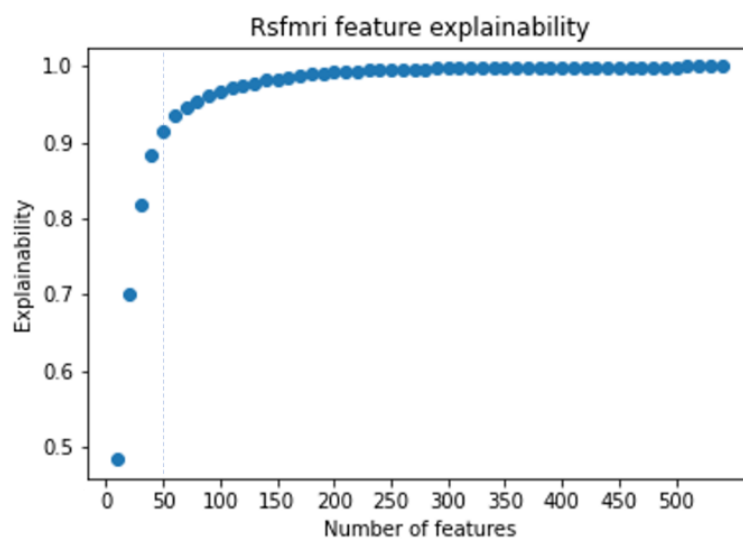
609

610 **Supplementary Table 4.** Top 10 features predictive of suicidal ideation. The models  
611 were trained on brain imaging-derived phenotypes and psychosocial data

Psychosocial		Structural MRI		Diffusion MRI		Resting state fMRI	
Feature	Importance	Feature	Importance	Feature	Importance	Feature	Importance
Internalizing-externalizing comorbidity	15.15	Anxiety / Depression	10.18	Internalizing-externalizing comorbidity	12.8	Depression	6.02
Prodromal psychosis_frequency	7.37	Prodromal psychosis_distress	6	Prodromal psychosis_frequency	7	Prodromal psychosis_frequency	5.33
Prodromal psychosis_distress	6.68	Family temper	3.71	Prodromal psychosis_distress	6.05	Withdrawn / Depressed	3.18
Family conflict	5.53	Family anger	3.22	Family anger	3.45	Obsessive-Compulsive Disorder(OCD)	2.56
Anxiety / Depression	3.38	Oppositional Defiant Disorder	3.07	Behavioral inhibition system	3.23	Weight	2.44
Depression	3.01	Externalizing disorder	3.05	Rash tendency in extreme	2.72	Internal comorbidity	2.39
Family angry	2.65	ADHD	2.68	Connectivity_Right-Hippocampus_Gray matter of right transverse temporal gyrus	2.65	Social Problems	2.11
Family peace	2.57	Sex	2.54	Depression	2.61	Married	2.1
Income	2.35	Internal comorbidity	2.52	Aggressive behavior	2.56	Family Angry	1.97
Internal comorbidity	2.2	Total Problem	2.46	Family temper	2.12	Connectivity_retrosplenialtemporal_dorsalattention	1.92
		Stop signal task fMRI		N-back task fMRI		Monetary incentive delayed task fMRI	
		Feature	Importance	Feature	Importance	Feature	Importance
		Depression	9.19	Prodromal psychosis_frequency	10.77	Prodromal psychosis_frequency	9.75
		Prodromal psychosis_frequency	6.41	Anxiety / Depression	6.12	Aggressive Behavior	7.35
		Externalizing disorder	5.74	Externalizing disorder	5.37	Prodromal psychosis_distress	7.04
		Prodromal psychosis_distress	5.55	Aggressive behavior	3.71	Obsessive-Compulsive Disorder(OCD)	6.4
		Internal comorbidity	5.3	Rule breaking behavior	3.4	Depression	5.51
		Family anger	3.27	Depression	3.1	Internalizing-externalizing comorbidity	4.76
		Anxiety / Depression	2.75	Internalizing-externalizing comorbidity	2.8	superior frontal gyrus (L)	2.74
		Internalizing-externalizing comorbidity	2.53	Family conflict	2.47	Externalizing disorder	2.64
		Obsessive-Compulsive Disorder(OCD)	2.39	Conduct disorder	2.43	Family temper	2.16
		Race	1.85	Obsessive-Compulsive Disorder(OCD)	2.41	middle temporal gyrus (L)	9.75

612

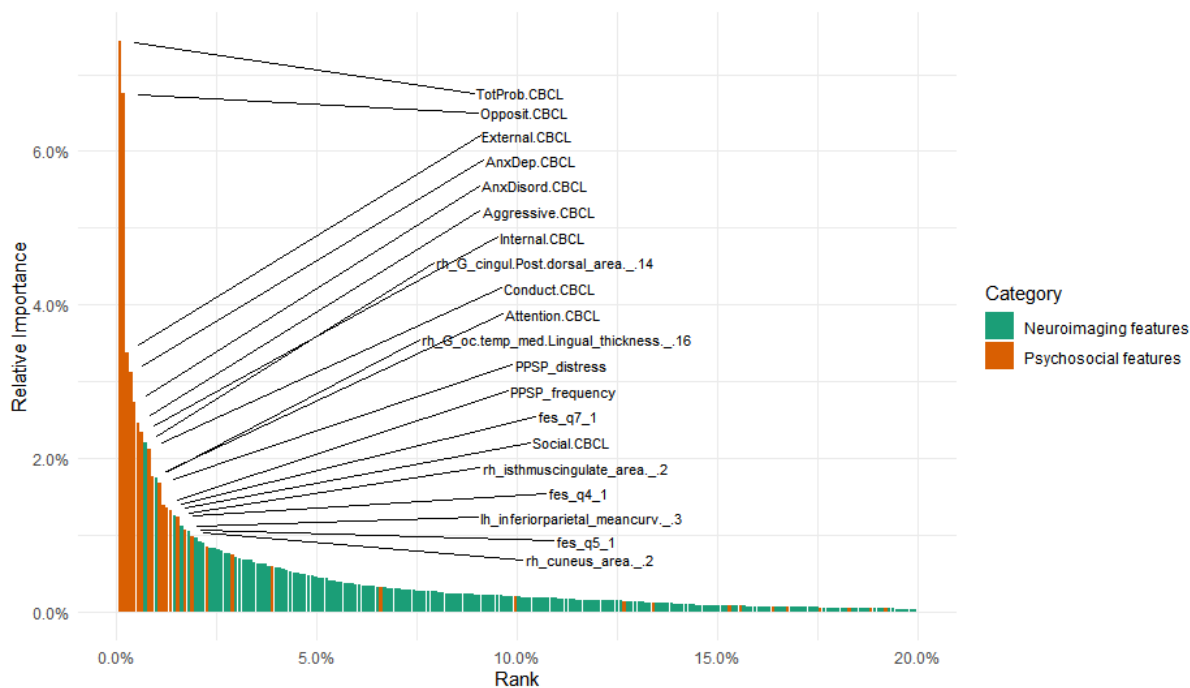
613 **Supplementary Figure 1. Explainability of the resting-state fMRI combined model**  
614 **as an increase of the number of features.** Top 50 features contain explainability of 91.6%.



615

616 **Supplementary Figure 2. Feature importance plots of combined models.** Top 20 features  
 617 are denoted.

618 (A) Structural MRI



619

Aggressive.CBCL	Aggressive behavior
AnxDep.CBCL	Anxious/Depressed behavior
AnxDisord.CBCL	Anxious behavior
Attention.CBCL	Attention problems
Conduct.CBCL	Conduct problems
cuneus_area	Cuneus area
External.CBCL	Externalizing behavior
fes_q4_1	Family conflict_losing tempers
fes_q5_1	Family conflict_criticizing
fes_q7_1	Family_reconciliation attempt
G_cingul.Post.dorsal_area	Posterior-dorsal part of the cingulate gyrus
G_oc.temp_med.Lingual_thickness	Lingual gyrus thickness
inferiorparietal_meancurv	Inferior-parietal mean curve
Internal.CBCL	Internalizing behaviour
isthmuscingulate_area	Isthmus cingulate area
Opposit.CBCL	OCD problem
PPSP_distress	Prodromal psychosis_distress
PPSP_frequency	Prodromal psychosis_frequency

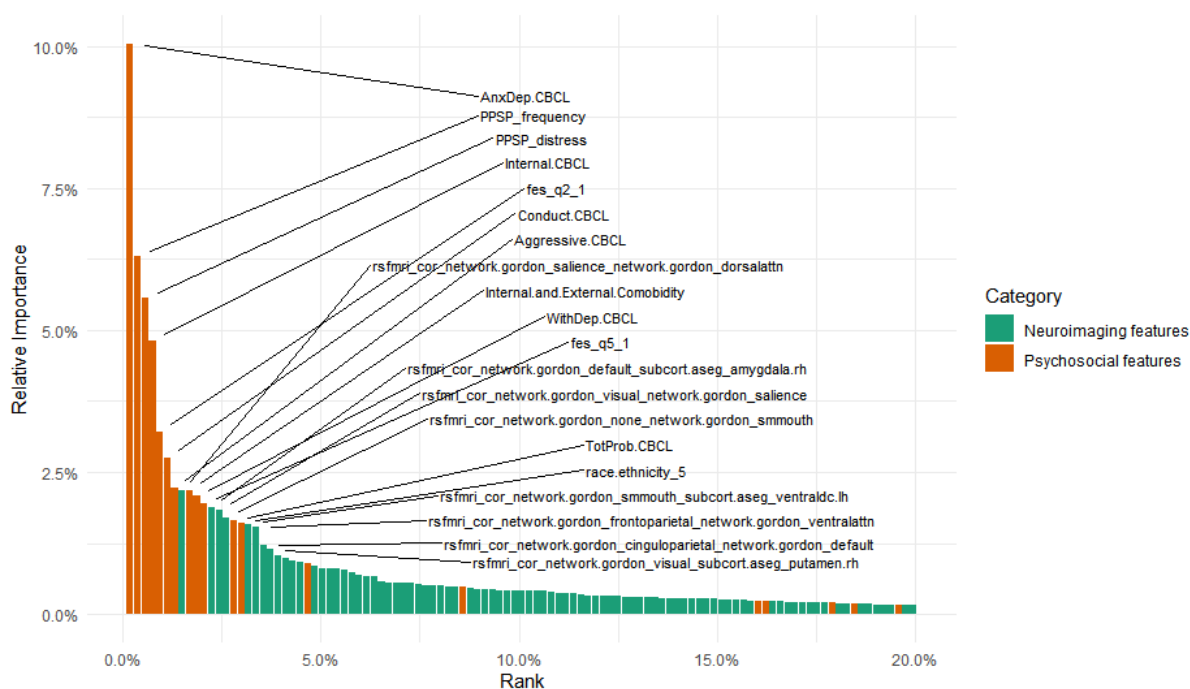
Social.CBCL	Social problems
TotProb.CBCL	Total behavioral problems

620

621

622

623 (B) Resting state functional MRI



624

AnxDep.CBCL	Anxious/Depressed behavior
Aggressive.CBCL	Aggressive behavior
cinguloparietal	Cingulo parietal
Conduct.CBCL	Conduct problems
cor_network	Correlation between two networks
dorsalattn	Dorsal attention
fes_q2_1	Family conflict_openly angry
fes_q5_1	Family conflict_criticism
Internal.and.External.Comobidity	Internalizing and Externalizing behavior
Internal.CBCL	Internalizing behaviour
PPSP_distress	Prodromal psychosis_distress
PPSP_frequency	Prodromal psychosis_frequency
race.ethnicity	Race/ethnicity

smmouth	Somatomotor cortex to the mouth
TotProb.CBCL	Total behavioral problems
ventralattn	Ventral attention
ventraldc	Ventral DC
WithDep.CBCL	Withdrawn/Depressed behavior

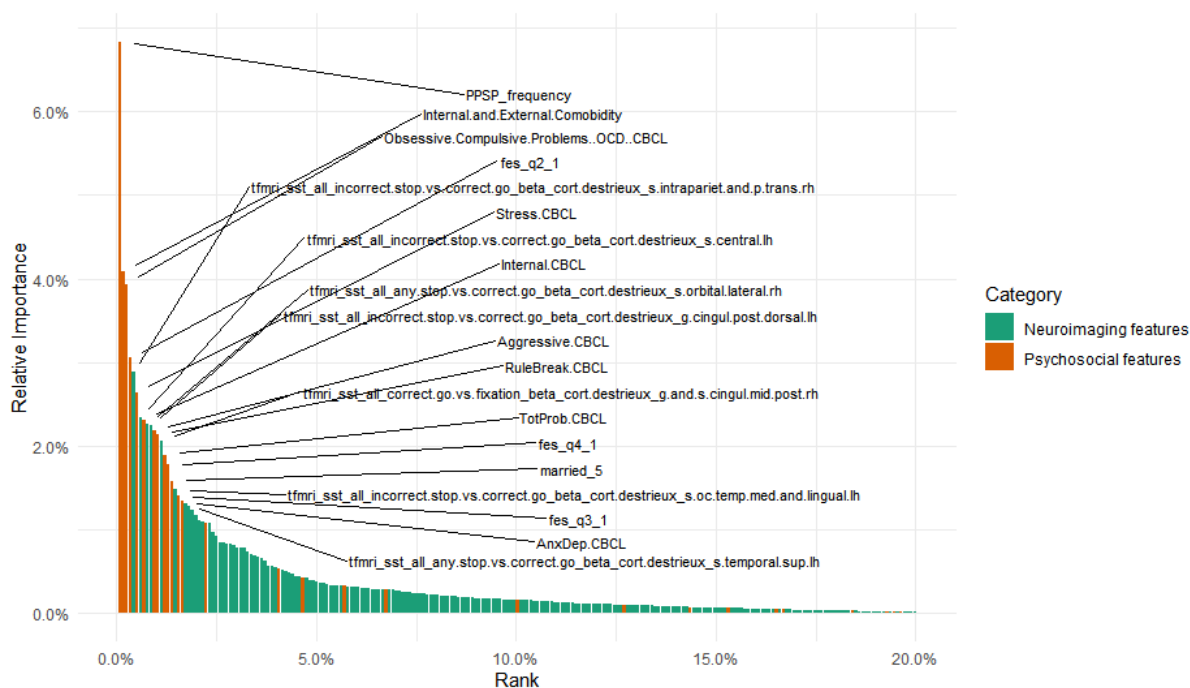
625

626

627

628

629 (C) Stop signal task functional MRI



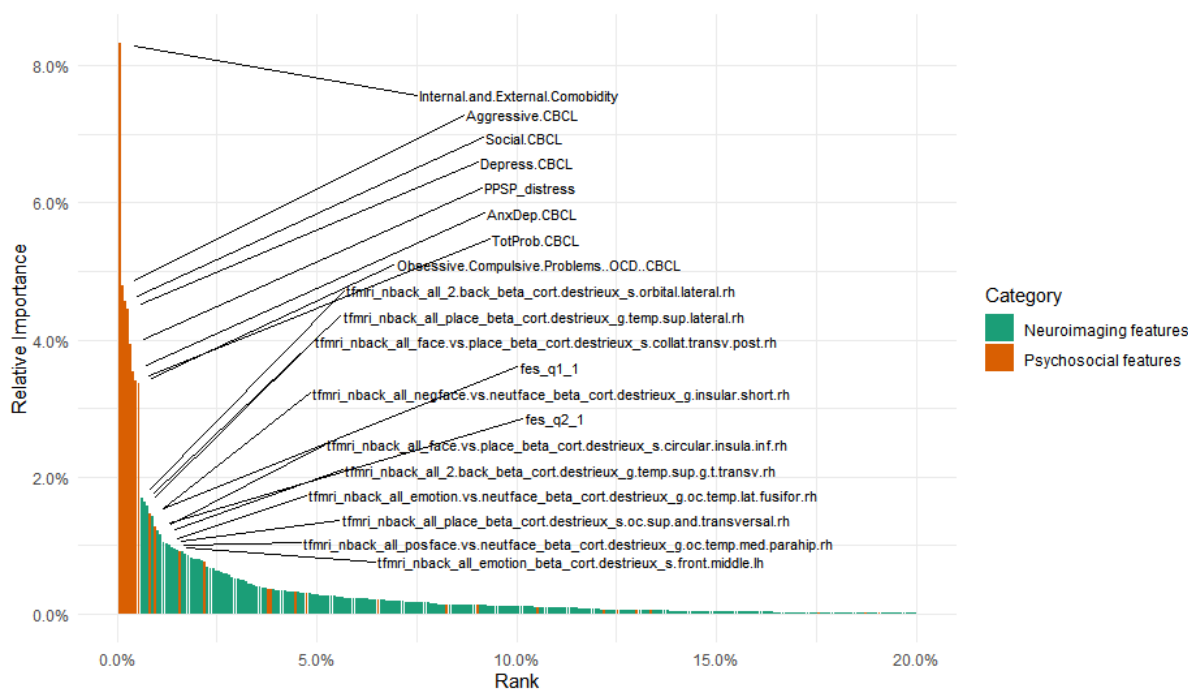
630

Aggressive.CBCL	Aggressive problem
AnxDep.CBCL	Anxious/depressed behavior
fes_q2_1	Family conflict_openly angry
fes_q3_1	Family conflict_throwing things
fes_q4_1	Family conflict_losing tempers
g.and.s.cingul.mid.post	Middle-posterior part of the cingulate gyrus and sulcus
s.central	Central sulcus
g.cingul.post.dorsal	Posterior-dorsal part of the cingulate gyrus

Internal.and.External.Comorbidity	Internalizing and Externalizing behavior
Internal.CBCL	Internalizing behaviour
married	Never married
Obsessive.Compulsive.Problems..OCD..CBCL	OCD problems
PPSP_frequency	Prodromal psychosis_distress
RuleBreak.CBCL	Rule breaking problem
s.intrapariet.and.p.trans	Intraparietal sulcus and transverse parietal sulci
s.oc.temp.med.and.lingual	Medial occipito-temporal sulcus and lingual sulcus
s.orbital.lateral	Lateral orbital sulcus
s.temporal.sup	Superior temporal sulcus
Stress.CBCL	Stress problems
TotProb.CBCL	Total behavioral problem

631

632 (D) Emotional N-back functional MRI



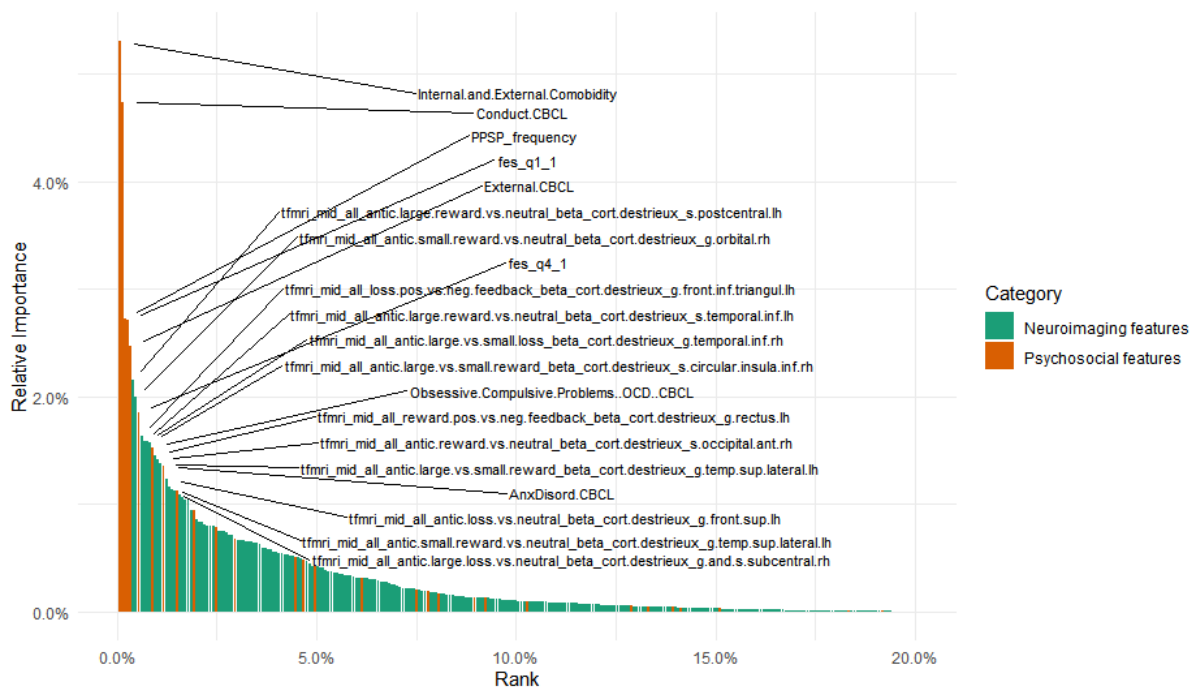
633

tfmri	Task functional mri
nback	Emotional N-back functional mri
Aggressive.CBCL	Aggressive problem
AnxDep.CBCL	Anxious/depressed behavior
Depress.CBCL	Depression problems
fes_q1_1	Family_frequent fights
fes_q2_1	Family conflict_openly angry

g.insular.short	short insular gyri
g.oc.temp.lat.fusifor	lateral occipito-temporal gyrus
g.oc.temp.med.parahip	parahippocampal gyrus
g.temp.sup.g.t.transv	anterior transverse temporal gyrus
g.temp.sup.lateral	lateral aspect of the superior temporal gyrus
Internal.and.External.Comobidity	Internalizing and Externalizing behavior
Obsessive.Compulsive.Problems..OCD..CBCL	OCD problems
PPSP_distress	Prodromal psychosis_distress
s.circular.insula.inf	Inferior segment of the circular sulcus of the insula
s.collat.transv.post	Posterior transverse collateral sulcus
s.front.middle	Middle frontal sulcus
s.oc.sup.and.transversal	Superior occipital sulcus and transverse occipital sulcus
Social.CBCL	Social problems
s.orbital.lateral.rh	Lateral orbital sulcus (right hemisphere)
TotProb.CBCL	Total behavioral problems

634

635 (E) Monetary incentive delay functional MRI



636

AnxDisord.CBCL	Anxious behavior
Conduct.CBCL	Conduct problems
External.CBCL	Externalizing behavior
fes_q1_1	Family_frequent fights
fes_q4_1	Family conflict_losing tempers
g.and.s.subcentral.rh	Subcentral gyrus and sulci (right hemisphere)

g.front.inf.triangul.lh	Triangular part of the inferior frontal gyrus (left hemisphere)
g.front.sup.lh	Superior frontal gyrus (left hemisphere)
g.orbital.rh	Orbital gyri (right hemisphere)
g.rectus.lh	Gyrus rectus (left hemisphere)
g.temporal.inf.rh	Inferior temporal gyrus (right hemisphere)
g.temp.sup.lateral.lh	Lateral aspect of the superior temporal gyrus (left hemisphere)
Internal.and.External.Comorbidity	Internalizing and Externalizing behavior
Obsessive.Compulsive.Problems..OCD..CBCL	OCD problems
PPSP_frequency	Prodromal psychosis_distress
s.circular.insula.inf.rh	Inferior segment of the circular sulcus of the insula (right hemisphere)
s.occipital.ant.rh	Anterior occipital sulcus and preoccipital notch (right hemisphere)
s.postcentral.lh	Postcentral sulcus (left hemisphere)
s.temporal.inf.lh	Inferior temporal sulcus (left hemisphere)